Magneto-Inductive HF RFID System

Richard R. A. Syms, *Senior Member*, Oleksiy Sydoruk,
and Michael C. K. Wiltshire

***Abstract*—Efforts to increase read range in passive HF RFID systems are hampered by the poor range scaling law of inductive coupling. An alternative approach to enlarging capture volume—increasing the lateral extent of the antenna—is proposed, using a magneto-inductive (MI) travelling wave arrangement to allow larger antenna sizes. A theory of load modulation in MI systems is first presented, together with field simulations in the capture volume. A 2.3 metre-long MI antenna is then constructed, and an active tag emulator is used to demonstrate load modulation. RFID is then demonstrated, with the antenna in both reflection and transmission modes, using a custom reader constructed from laboratory equipment. A transverse read range of 0.5 m is obtained using commercial off-the-shelf RFID cards with 12 W RF power, with high uniformity along the length of the antenna.**

***Index Terms*—Magneto-inductive waveguide, Near-field communication, RFID, Travelling wave antenna**

I. Introduction

RADIOFREQUENCY identification (RFID) and related near-field communication (NFC) are technologies for wireless personal area networks [1], [2]. The widely used ISO/IEC 14443 standard sets operation in the industrial, scientific and medical band [3]. Readers use inductive coupling to power transponders at a frequency $f_0 = 13.56$ MHz. For Type A systems, reader queries are transmitted in modified Miller code on sub-carriers separated by $f_0/16 = 847$ kHz from f_0 using close to 100% amplitude shift key (ASK) at $f_0/128 = 106$ kB/s. Data is returned from transponders, using Manchester code with on-off-key (OOK) sub-carrier load modulation. To increase currents flowing in the antennas, reader and transponder antennas are both resonant. However, due to the large side-band separation, the reader coil must be loaded with resistors to reduce its Q-factor (typically, to around 20). Power transfer is maximized when the reader and transponder coils have their axes parallel and aligned, and falls off rapidly as orientation and position alter. The range scaling law is highly adverse; RF powers must increase with the sixth power of distance at long range, quickly leading to saturation in the receiver [4]. Efforts to increase transverse range have focused on the use of larger amplifiers and more effective filters in the receive chain [5], [6], battery powered transponders and separate transmit (TX) and receive (RX) antennas [7] or higher harmonics for RX [8]. Despite some success, diminishing returns are quickly obtained. Table I compares read ranges and power requirements for these works.

The authors are with the Department of Electrical and Electronic Engineering, Imperial College London, London, SW7 2AZ, United Kingdom (e-mail: r.syms@imperial.ac.uk).

TABLE I
Properties of RFID Tags Used in System Evaluation

Author	Ref	Technique	Range [m]	Power [W]
Kirschenbaum	[5]	Resonant antenna, attenuating buffer	0.25	NA
Zirbesegger	[6]	Resonant anteanna and and quartz crystal notch filter	0.16	NA
Finkenzeller	[7]	Separate resonant antennas, additional transponder	2.8	50
Habraken	[8]	Separate resonant antennas, higher harmonics	0.5	60
This work		Travelling wave antenna and filter coupler	0.5	12

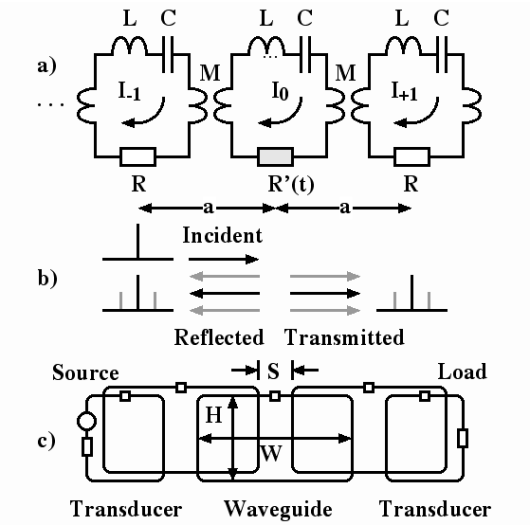

Fig. 1. a) Equivalent circuit of a magneto-inductive waveguide, b) mechanism of load modulation and c) arrangement of experimental antenna, with broadband transducers at source and load.

Here we consider an alternative approach to improving capture volume, increasing the lateral extent of the antenna. The perimeter lengths of loop antennas must be kept well below a wavelength to maintain current uniformity. However, lateral extent can be increased using a subdivided antenna in the form of a set of magnetically coupled L-C resonators, known as a magneto-inductive (MI) waveguide [9]–[11] and shown in Fig. 1a. The resonant loops can be arranged in the so-called axial or planar configurations, leading to positive or negative values of the mutual inductance M and allowing propagation of forward or backward current waves, respectively. Careful design is required to ensure low losses. Despite this, applications for MI waves have been found in communications [12]–[14], power transfer [15]–[17] and sensing [18]–[20].

A magneto-inductive wave can clearly generate an extended magnetic field around such an antenna. Modulation of the load in one element (for example, element zero) by a transponder will give rise to reflected and transmitted waves at the carrier and sideband frequencies, as shown in Fig. 1b. These waves

will propagate to the ends of the antenna, where they may be detected. Thus, a MI waveguide can provide multiple opportunities to power and read a tag at different positions. Although (as we show) higher RF power is required for a given transverse range than using a single antenna, the RF power is largely unaffected by the length of the antenna. The approach may therefore prove useful in applications involving a steady flow of traffic or goods. In Sec. II, we develop a simple theory for load modulation in magneto-inductive systems, and present field simulations that highlight the increased capture volume. In Sec. III, we describe construction of a prototype traveling wave antenna, and make a first demonstration of load modulation of MI waves. In Sec. IV, we describe a full RFID reader based on a MI antenna and laboratory equipment. Conclusions are presented in Sec. V.

II. Load modulation: Theory

We first explain the principle of load modulation for magneto-inductive waves. We base the analysis on the equivalent circuit model shown in Fig. 1a. Here L-C resonators with associated resistance R are magnetically coupled to nearest neighbours via mutual inductance M. In element zero we assume load modulation at angular frequency $\omega_{\rm m}$. Without loss of generality we assume the modulation is resistive, so the resistance of this element varies with time as

$$R'(t) = R + \Delta R_0 + \Delta R_1 \cos(\omega_{\rm m} t)\,. \tag{1}$$

Here ΔR_0 and ΔR_1 are DC and AC modulation amplitudes, and the DC term is required to ensure the modulation is always lossy. The circuit equation for element zero is then

$$L\frac{dI_0}{dt} + R' I_0 + \frac{1}{C}\int I_0 dt + M\left(\frac{dI_{-1}}{dt} + \frac{dI_{+1}}{dt}\right) = 0\,. \tag{2}$$

Here I_n is the $n^{\rm th}$ element current. In the other elements, we need only solve the simpler equation

$$L\frac{dI_n}{dt} + RI_n + \frac{1}{C}\int I_n dt + M\left(\frac{dI_{n-1}}{dt} + \frac{dI_{n+1}}{dt}\right) = 0\,. \tag{3}$$

We now assume a current wave at angular frequency ω is incident from the left. Standard physics suggests that there will be transmitted and reflected waves, not only at ω but also at the lower and upper side-band frequencies $\omega_- = \omega - \omega_{\rm m}$ and $\omega_+ = \omega + \omega_{\rm m}$. These terms all propagate as MI waves. We therefore assume solutions in the form of a set of travelling waves, as

$$\begin{aligned} I_n(t) =& \frac{1}{2}\left\{\left[A_{\rm I} e^{j\omega t} e^{-jnka} + {\rm cc}\right] + \left[A_{\rm R-} e^{j\omega_- t} e^{jnk_- a} + {\rm cc}\right]\right. \\ &\left. + \left[A_{\rm R} e^{j\omega t} e^{jnka} + {\rm cc}\right] + \left[A_{\rm R+} e^{j\omega_+ t} e^{jnk_+ a} + {\rm cc}\right]\right\} \\ &\text{for } n \le 0 \\ I_n(t) =& \frac{1}{2}\left\{\left[A_{\rm T} e^{j\omega t} e^{-jnka} + {\rm cc}\right] + \left[A_{\rm T-} e^{j\omega_- t} e^{-jnk_- a} + {\rm cc}\right]\right. \\ &\left. + \left[A_{\rm T+} e^{j\omega_+ t} e^{-jnk_+ a} + {\rm cc}\right]\right\} \\ &\text{for } n > 0\,. \end{aligned} \tag{4}$$

Here $A_{\rm I}$ is the amplitude of the incident wave, $A_{\rm R}$, $A_{\rm R-}$ and $A_{\rm R+}$ are the amplitudes of the reflected carrier and the two sidebands, $A_{\rm T}$, $A_{\rm T-}$ and $A_{\rm T+}$ are the amplitudes of the transmitted carrier and sidebands and 'cc' denotes complex conjugate. Similarly, k, k_- and k_+ are the propagation constants at the carrier and side-band frequencies, respectively, and a is the period of the waveguide. Substituting into Eq. (2), equating the coefficients of $\exp(\pm j\omega t)$, $\exp(\pm j\omega_- t)$ and $\exp(\pm j\omega_+ t)$ separately with zero and ignoring other frequencies we obtain

$$\begin{aligned} &\left(R + \Delta R_0 + j\omega L + \frac{1}{j\omega C}\right)(A_{\rm I} + A_{\rm R}) \\ &+ \frac{\Delta R_1}{2}(A_{\rm R-} + A_{\rm R+}) \\ &+ j\omega M\left(A_{\rm I} e^{jka} + A_{\rm R} e^{-jka} + A_{\rm T} e^{-jka}\right) = 0 \\ &\left(R + \Delta R_0 + j\omega_- L + \frac{1}{j\omega_- C}\right) A_{\rm R-} + \frac{\Delta R_1}{2} A_{\rm I} \\ &+ j\omega_- M\left(A_{\rm R-} e^{jk_- a} + A_{\rm T-} e^{-jk_- a}\right) = 0 \\ &\left(R + \Delta R_0 + j\omega_+ L + \frac{1}{j\omega_+ C}\right) A_{\rm R+} + \frac{\Delta R_1}{2} A_{\rm I} \\ &+ j\omega_+ M\left(A_{\rm R+} e^{jk_+ a} + A_{\rm T+} e^{-jk_+ a}\right) = 0\,. \end{aligned} \tag{5}$$

Analogous equations are obtained for complex conjugate terms. Note that higher harmonics exist at frequencies of the form $\omega_{2\pm} = \omega \pm 2\omega_{\rm m}$ and $\omega_{3\pm} = \omega \pm 3\omega_{\rm m}$ and so on. If these waves are retained in a more extensive analysis, the result is a larger set of simultaneous equations that can be solved numerically to determine the wave amplitudes. Here, we focus on the smallest number of harmonics, and assume that even these terms have small amplitude so that the fundamental is un-depleted. This approach provides a useful qualitative description of the basic phenomena and yields simple analytic solutions.

Carrying out similar manipulations using Eq. (3), for $n = 1$, we get

$$\begin{aligned} &\left(R + j\omega L + \frac{1}{j\omega C}\right) A_{\rm T} e^{-jka} \\ &+ j\omega M\left(A_{\rm I} + A_{\rm R} + A_{\rm T} e^{-2jka}\right) = 0 \\ &\left(R + j\omega_- L + \frac{1}{j\omega_- C}\right) A_{\rm T-} e^{-jk_- a} \\ &+ j\omega_- M\left(A_{\rm R-} + A_{\rm T-} e^{-2jk_- a}\right) = 0 \\ &\left(R + j\omega_+ L + \frac{1}{j\omega_+ C}\right) A_{\rm T-} e^{-jk_+ a} \\ &+ j\omega_+ M\left(A_{\rm R+} + A_{\rm T+} e^{-2jk_+ a}\right) = 0\,. \end{aligned} \tag{6}$$

Other values of n yield only the dispersion equation for MI waves, namely [9], [11]

$$R + j\omega L + \frac{1}{j\omega C} + 2j\omega M\cos(ka) = 0\,. \tag{7}$$

Since Eq. (7) is complex, the propagation constant k must also be complex. Writing $k = k' - jk''$, and assuming that losses are low, so that $k'' \ll k'$, we may approximate Eq. (7) as

$$\begin{aligned} 1 - \frac{1}{\omega^2 LC} + 2\frac{M}{L}\cos(k'a) &\approx 0 \\ k''a &\approx \frac{R}{2\omega M \sin(k'a)} \end{aligned} \tag{8}$$

The upper equation is the dispersion relation for lossless MI waves. For positive M, this implies that propagation is band-limited to frequencies in the range $1/\sqrt{1+\kappa} \le \omega/\omega_0 \le 1/\sqrt{1-\kappa}$, where $\omega_0 = 1/\sqrt{LC}$ is the resonant frequency and $\kappa = 2M/L$ is the coupling coefficient. However, with strong coupling, bandwidth can be large, and easily sufficient to encompass RFID sidebands.

The lower equation gives the approximate variation of the attenuation coefficient. Losses are minimised at the resonant frequency, when $k'a = \pi/2$ and $k''a \approx R/(2\omega_0 M)$. For lossless systems, it is simple to show that the characteristic impedance is $j\omega M \exp(-jka)$. At resonance, this reduces to the real value $Z_{0\mathrm{M}} = \omega_0 M$, so the minimum value of $k''a$ is set by the ratio of resistive power loss to power flow. Low element resistance and high impedance are therefore required for low loss. However, $Z_{0\mathrm{M}}$ will normally be chosen to match the overall system impedance.

Similar relations are obtained between ω_+ and k_+ and between ω_- and k_-. Using these together, Eq. (5) can be reduced to

$$\begin{aligned} &\Delta R_0(A_\mathrm{I} + A_\mathrm{R}) + \frac{\Delta R_1}{2}(A_{\mathrm{R}-} + A_{\mathrm{R}+}) \\ &+ j\omega M\left(-A_\mathrm{I}e^{-jka} - A_\mathrm{R}e^{jka} + A_\mathrm{T}e^{-jka}\right) = 0 \\ &\Delta R_0 A_{\mathrm{R}-} + \frac{\Delta R_1}{2}A_\mathrm{I} \\ &+ j\omega_- M\left(-A_{\mathrm{R}-}e^{jk_-a} + A_{\mathrm{T}-}e^{-jk_-a}\right) = 0 \\ &\Delta R_0 A_{\mathrm{R}+} + \frac{\Delta R_1}{2}A_\mathrm{I} \\ &+ j\omega_+ M\left(-A_{\mathrm{R}+}e^{jk_+a} + A_{\mathrm{T}+}e^{-jk_+a}\right) = 0\,. \end{aligned} \tag{9}$$

In a similar way, Eq. (6) can be reduced to relations between the wave amplitudes, in the form $A_\mathrm{I} + A_\mathrm{R} = A_\mathrm{T}$, $A_{\mathrm{R}-} = A_{\mathrm{T}-}$ and $A_{\mathrm{R}+} = A_{\mathrm{T}+}$. Assuming now that $A_{\mathrm{R}-}$ and $A_{\mathrm{R}+}$ are small, and using the relations above to simplify Eq. (9), we obtain

$$\begin{aligned} \frac{A_\mathrm{R}}{A_\mathrm{I}} &= \frac{-\Delta R_0}{\Delta R_0 + 2\omega M \sin(ka)} \\ \frac{A_{\mathrm{R}\pm}}{A_\mathrm{I}} &= \frac{A_{\mathrm{T}\pm}}{A_\mathrm{I}} = \frac{-\Delta R_1}{2\left[\Delta R_0 + 2\omega_\pm M \sin(k_\pm a)\right]} \end{aligned} \tag{10}$$

These results imply that the effect of the static load modulation is simply to reflect the carrier. However, the time-varying part excites harmonic waves, which travel with equal amplitudes in opposite directions. Because of the term $\omega_\pm$ in the denominator, the lower and upper sideband amplitudes are not identical, but tend to each other as ω_m tends to zero. Normally, the carrier will be chosen to lie at the resonant frequency ω_0. Assuming further that $\Delta R_1 \approx \Delta R_0$, and that the sideband frequencies are close to ω_0, the results above tend to $A_\mathrm{R}/A_\mathrm{I} = -\Delta R_1/2Z_{0\mathrm{M}}$ and $A_{\mathrm{R}\pm}/A_\mathrm{I} = A_{\mathrm{T}\pm}/A_\mathrm{I} = -\Delta R_1/4Z_{0\mathrm{M}}$. Thus, the important aspect is the amplitude of the load modulation relative to the characteristic impedance.

We now consider the capture volume. Fig. 1c shows a suitable arrangement for an MI antenna with positive M is based on overlapping rectangular loops. This format has previously been used to obtain low loss in flexible cable [21], and the use of terminating elements with half the loop length allows broadband coupling to resistive loads [22]. The external magnetic field it produces may be modelled by combining standard field solutions for a single rectangular loop [23], [24]. For example, for a loop lying the x-y plane, centred on the point $(0,0,0)$ and with side dimensions measuring W (in the x-direction) and H (in the y-direction), the components of the magnetic field at a general point (x,y,z) are

$$\begin{aligned} H_x &= \frac{I}{4\pi}\sum_{n=1}^{4}\frac{(-1)^{n+1}z}{r_n(r_n+d_n)} \\ H_y &= \frac{I}{4\pi}\sum_{n=1}^{4}\frac{(-1)^{n+1}z}{r_n\left(r_n+(-1)^{n+1}c_n\right)} \\ H_z &= \frac{I}{4\pi}\sum_{n=1}^{4}\left[\frac{(-1)^n d_n}{r_n(r_n+(-1)^{n+1}c_n)} - \frac{c_n}{r_n(r_n+d_n)}\right] \end{aligned} \tag{11}$$

Here the coefficients c_n, d_n and r_n are given by

$$\begin{aligned} c_1 = -c_4 &= W/2 + x \\ c_2 = -c_3 &= W/2 - x \\ d_1 = d_2 &= y + H/2 \\ d_3 = d_4 &= y - H/2 \\ r_1 &= \sqrt{(W/2+x)^2 + (y+H/2)^2 + z^2} \\ r_2 &= \sqrt{(W/2-x)^2 + (y+H/2)^2 + z^2} \\ r_3 &= \sqrt{(W/2-x)^2 + (y-H/2)^2 + z^2} \\ r_4 &= \sqrt{(W/2+x)^2 + (y-H/2)^2 + z^2} \end{aligned} \tag{12}$$

To model the external field of the full set of loops comprising a travelling wave antenna, all that is required is to combine such solutions, taking into account the position of each loop and the phase of the current it carries. As an example, to match later experiments, we assume loops of width $W = 1$ m and height $H = 0.35$ m, arranged with a period of $a = 0.57$ m, and operating at resonance when adjacent loop currents are in quadrature. Figs. 2a, b and c show the spatial variations of the moduli of the magnetic field components H_x, H_y and H_z for a section of uniform guide, calculated at a distance $z = 0.5$ m, together with an indicative representation of the antenna elements. Peaks in H_y are narrow, and mainly align with the horizontal conductors. The two strongest components

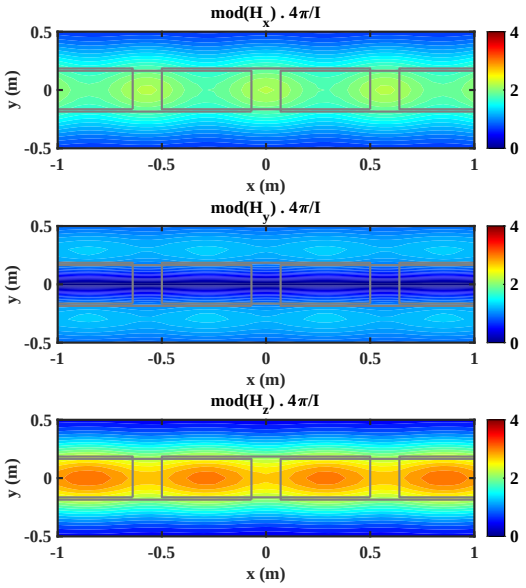

Fig. 2. a) External magnetic fields of a magneto-inductive waveguide, in the cable configuration: a) H_x, b) H_y, and c) H_z, calculated at $z = 0.5$ m assuming $W = 1$ m, $H = 0.35$ m and $a = 0.57$ m. Superimposed grey lines indicate antenna element positions behind, offset for clarity.

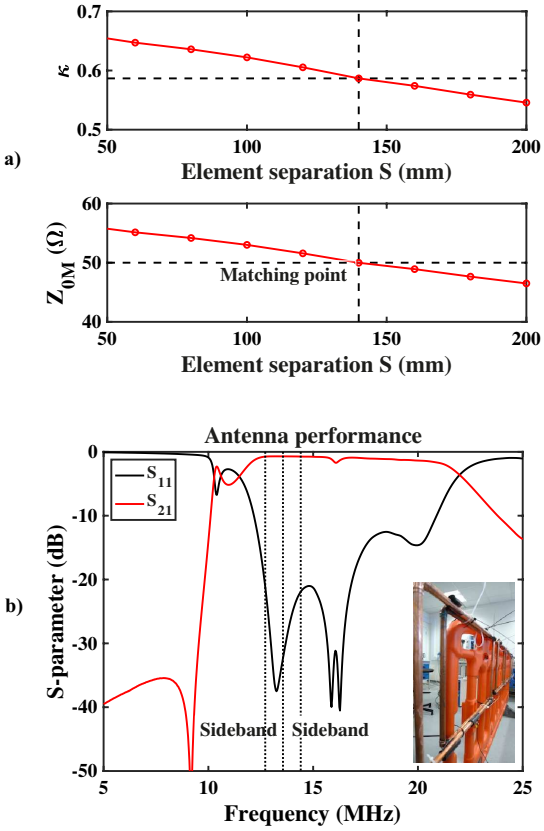

Fig. 3. a) Variation of coupling coefficient κ and characteristic impedance Z_{0M} with element separation S; b) variation of antenna S-parameters with frequency, with inset antenna.

are H_x and H_z; peaks in the transverse field H_z are broad, lie at the centre of each overlap region, and alternate with similar peaks in H_x. These two field components therefore provide an extended capture volume for suitably oriented tags.

III. Load Modulation: Experiment

We now perform an experimental demonstration of load modulation. The complete waveguide contained five loops and comprised three main loops and a pair of coupling transducers as shown in Fig. 1c. Each loop was constructed from 15 mm diameter copper pipe soldered to pipe bends, with an insulated gap to allow component attachment. Each main loop had $W = 1$ m and $H = 0.35$ m, giving an inductance $L \approx 2\mu$H. Resonance at $f_0 = 13.56$ MHz was achieved using mica capacitors, and measurements using uncalibrated inductive probes and a network analyser (Keysight E5061B) gave Q-factors > 300 without de-embedding, but using very weak coupling to avoid loading effects. Each coupling transducer was of width $W/2$ and inductance $L/2$, requiring twice the capacitance for resonance. This capacitance was split to float the antenna.

The separation S was determined experimentally. A coupled resonator was first constructed by mounting a pair of elements on a dielectric support, in the nearest neighbour configuration. The coupling coefficient was estimated from values of the two resonant frequencies $\omega_{1,2} = 1/\sqrt{(L \pm M)C}$ determined using inductive probes. Fig. 3a shows the variation of κ with element separation S; values greater than 0.55 are obtained for separations S up to 200 mm. In this regime, the second-neighbour coupling coefficient was negligible. Fig. 3a also shows the variation of the characteristic impedance Z_{0M}, which implies that matching to 50 Ω will be obtained with $S = 140$ mm, when $\kappa \approx 0.59$. At this point, the period is $a = (W + S)/2 = 0.57$ m. This result suggests that low-loss propagation will be obtained, with $k''a \approx 1/(300 \times 0.59)$, corresponding to a power loss of 0.05 dB/element.

A full antenna was then constructed on a high-density polyethylene dielectric support with this separation, and the transducer positions were adjusted for optimum power transfer, giving an overall length of 2.3 m. Such a large antenna would require wall-mounting, and care would be needed to avoid coupling to nearby metallic structures such as reinforcement rods. Fig. 3b shows the frequency dependence of the S-parameters of the completed antenna, with the dotted lines marking the frequencies of the carrier and sidebands and an inset showing the antenna itself. Low-loss transmission is obtained over an extremely broad band, between around 10 and 20 MHz, with the -10 dB bandwidth extending almost to 24 MHz. The minimum transmission loss is -0.7 dB, or 0.14 dB/element; the excess over the theoretical prediction is attributed to residual impedance mismatch. Reflection is minimised at f_0, and also near the higher frequency $f_0/(1 - \kappa^2) \approx 1.25 f_0$ predicted from the theory of broadband transducers [22], with a wide band of approximate matching between these values.

Load modulation was demonstrated using the tag emulator shown in Fig. 4a. An inductive loop L_1 with associated resistance R_1 formed on a large printed circuit board was first matched and tuned for 50 Ω impedance at 13.56 MHz

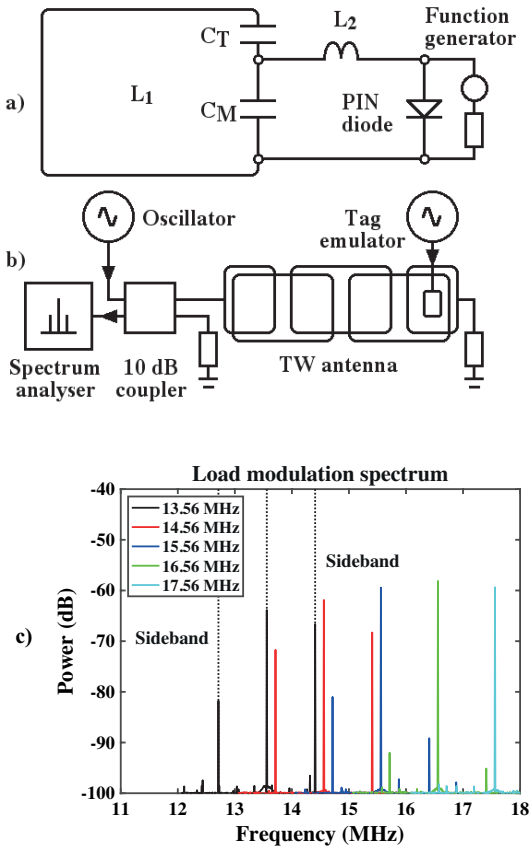

Fig. 4. a) Active tag emulator, b) arrangement for demonstration of load modulation, and c) modulation spectrum, for carrier frequencies of 13.56, 14.56, 15.56, 16.56 and 17.56 MHz.

frequency using capacitors C_M and C_T. These components were chosen to satisfy the standard relationships $\omega_0 C_M = 1/\sqrt{Z_0 R_1}$ and $1/C_T + 1/C_M = 1/C_{eff}$, where $\omega_0 = 1/\sqrt{L_1 C_{eff}}$, with $Z_0 = 50\ \Omega$ and $f_0 = \omega_0/(2\pi) = 13.56$ MHz. An inductor L_2 formed from a length of short-circuited co-axial cable was then tuned to resonate with C_M. The short circuit was then replaced with a shunt-connected PIN diode (M/A-COM Technology Solutions MA4P7464 F-1072) and a control cable to a function generator (TTi TGA 1244). With the diode in reverse bias, the loop was resonant, with a loaded Q-factor of 31. In forward bias, the tank filter formed by C_M and L_2 split the resonance, inserting large impedance into the loop at f_0. This simple arrangement allowed continuous load modulation, over a wide bandwidth.

Load modulation experiments were performed as shown in Fig. 4b. An oscillator (Agilent N5181A) provided a carrier, which was injected into the antenna via a lumped-element 10 dB coupler and absorbed in a load at the far end. The tag emulator was driven with a sinusoidal voltage at 847 kHz frequency. Signals were detected from the unused coupler input with a spectrum analyser (Agilent N1996A). The black line in Fig. 4c shows the frequency spectrum obtained with the tag emulator at the far end of the antenna and the carrier at 13.56 MHz frequency. Sidebands are clearly present at the expected frequencies. Similar results were obtained with the tag at alternative positions along the antenna, and

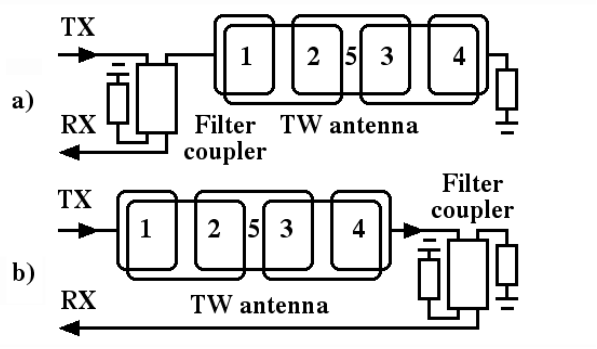

Fig. 5. Arrangement of travelling wave antenna, with signal reception in a) reflection and b) transmission.

at different carrier frequencies. For example, the coloured lines show the result obtained at frequencies of 14.56, 15.56, 16.56 and 17.56 MHz. There is a systematic change in the average and relative values of the sideband amplitudes with carrier frequency, with the largest and most equal values being obtained at 14.56 MHz. This behaviour may be attributed to the narrow bandwidth of the tag emulator, combined with slight detuning. The ability of non-resonant antenna to support load modulation over a wide bandwidth may prove useful in frequency-tuneable systems designed to compensate for variations in tag resonance.

IV. Magneto-Inductive RFID System

RFID was demonstrated using a custom reader. Interrogation codes compliant with ISO/IEC 14443 Type A were generated using a personal computer, and passed to a function generator (TTi TGA 1244). Output from the function generator was used to modulate a carrier at 13.56 MHz derived from a signal generator (Agilent N5181A). TX signals thus obtained were amplified using a power amplifier (Minicircuits LZY-22+). Received signals were passed through filters to suppress residual carrier before detection using a digital storage oscilloscope, which acted as a signal acquisition buffer (Keysight InfiniVision DSOX024T). Digitised signals were passed back to the PC. Software filtering was used to extract sidebands, and tag responses were recovered by rectification, correlation and decoding.

Preliminary separation of carrier and sideband signals was performed using a filter coupler. Two antenna arrangements were investigated. In the first (Fig. 5a), RX signals were obtained in reflection, using a single-ended arrangement with the filter between the amplifier and the antenna. In the second (Fig. 5b), signals were obtained in transmission, with the amplifier directly connected to the antenna. This arrangement allowed a slight reduction in TX losses. The best results were obtained after processing each sideband and averaging the results.

Experiments were conducted using a commercial off-the-shelf (COTS) RFID tag mounted parallel to the antenna on a dielectric support. Read range was determined by correct recovery of the correct unique ID without errors in parity or block check code and was repeatable to within ± 1 cm at a

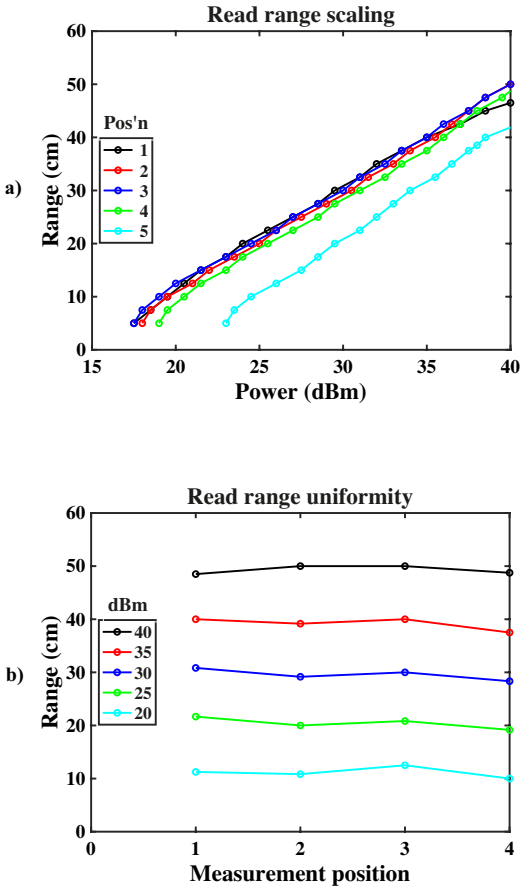

Fig. 6. Variation of read range a) with a RF power, at different tag positions, and b) with tag position, at different RF powers.

given RF power. Fig. 6a shows the variation of read range with TX power obtained in the transmission mode of Fig. 5b, with the tag placed at each of the positions labelled 1 to 5 in Fig. 5. A near-identical characteristic is obtained in each case, with a maximum transverse range of just over 0.5 m achieved at 10 W RF power. Range was slightly reduced (to 0.4 m) in positions such as 5, where the magnetic field is largely derived from currents flowing in a single loop rather than a pair of overlapping loops. Fig. 6b shows range data plotted as a function of measurement position, confirming the high degree of uniformity conferred by extremely low propagation loss. In fact, the measured attenuation data suggest that there would be little noticeable performance variation using an antenna of twice the length.

For a given RF power, currents in a magneto-inductive antenna are reduced in comparison with a single-loop resonator with internal resistance R by a factor $\sqrt{Z_{0\mathrm{M}}/R}$. However, for strongly overlapping loops in an MI waveguide operating at the design frequency, when adjacent currents are in quadrature, the external magnetic field is increased by $\sqrt{2}$. Consequently, the overall field reduction factor is $F = \sqrt{Z_{0\mathrm{M}}/(2R)}$. In other experiments with similar rectangular antennae, resistances $R \approx 5\ \Omega$ have been required to set an appropriate Q-factor. For $Z_{0\mathrm{M}} = 50\ \Omega$, we then obtain $F = \sqrt{5}$, implying that a 7 dB increase in power will be needed for similar transverse range in an MI system. We have verified this increase experimentally. The disadvantage is compensated by an increase in overall capture volume. In fact, once the capture volume has exceeded F^2 times that of a single loop, the travelling wave approach is more efficient. Other advantages may follow from the possibility of broadband operation in tuneable systems.

V. Conclusions

The principle of load modulation of magneto-inductive waves has been proposed and demonstrated. Its effect is to generate reflected and transmitted waves at side-band frequencies. Both can be detected easily, and (to first order) the result is independent of the position of the transponder. A travelling wave magneto-inductive antenna may therefore be used to form a near field communication system that allows multiple reading and writing opportunities over an extended volume. A complete RFID system has been constructed using a magneto-inductive antenna and a set of laboratory instruments. A transverse read range > 0.5 m for COTS RFID cards was obtained at an RF power of 10 W using a 2.3 metre-long antenna. The main limitation of the approach is clearly the bulk of the antenna, and a key challenge would be to explore lightweight, flexible and possibly printable alternatives to the rigid structures considered here. However, a long antenna may provide improved opportunities for tag reading in linear arrangements such as corridors or conveyor belts, especially when the tag range may vary due to natural motion. Advantages may also follow from the very large bandwidth, which in principle allows reading of widely detuned tags.

References

[1] K. Finkenzeller, *RFID Handbook*, 3rd ed. Chichester, UK: John Wiley and Sons, 2010.

[2] V. D. Hunt, A. Puglia, and M. Puglia, *RFID-A Guide to Radio Frequency Identification*. New York: John Wiley and Sons, 2007.

[3] ISO/IEC 14443, "Cards and security devices for personal identification—contactless proximity objects," International Organization for Standardization, Geneva, CH, Standard, 2018.

[4] W. Aerts, E. de Mulder, B. Preneel, G. A. E. Vendenbosch, and I. Verbauwhede, "Dependence of RFID reader antenna design on readout distance," *IEEE Trans. Antennas Propag.*, vol. 56, no. 12, pp. 3829–3837, 2008.

[5] I. Kirschenbaum and A. Wool, "How to build a low-cost, extended-range RFID skimmer," in *Proc. 15th USENIX Security Symp., Vancouver, CA, July 31-Aug 4*, 2006, pp. 43–57.

[6] J. Zirbesegger, M. Gebhart, E. Merlin, and E. Leitgeib, "Extending the analogue performance of integrated 13.56 MHz proximity chips," *Elektrotech. Inftech.*, vol. 124, pp. 369–375, 2007.

[7] K. Finkenzeller, F. Pfeiffer, and E. Biebl, "Range extension of an ISO/IEC 14443 type A RFID system with actively emulating load modulation," in *Proc. RFIDSysTech.'11, Dresden, Germany, May 17-18*, 2011.

[8] R. Habraken, P. Dolron, E. Poll, and J. de Ruiter, "An RFID skimming gate using higher harmonics," in *RFIDsec 2015, LNCS 9440*, S. Mangard and P. Schaumont, Eds., 2015, pp. 122–137.

[9] E. Shamonina, V. A. Kalinin, K. H. Ringhofer, and L. Solymar, "Magnetoinductive waves in one, two, and three dimensions," *J. Appl. Phys.*, vol. 92, pp. 6252–6261, 2002.

[10] E. Shamonina, V. Kalinin, K. Ringhofer, and L. Solymar, "Magneto-inductive waveguide," *Electron. Lett.*, vol. 38, no. 8, pp. 371–373, 2002.

[11] M. C. K. Wiltshire, E. Shamonina, I. R. Young, and L. Solymar, "Dispersion characteristics of magneto-inductive waves: comparison between theory and experiment," *Electron. Lett.*, vol. 39, pp. 215–217, 2003.

[12] C. J. Stevens, C. W. T. Chan, K. Stamatis, and D. J. Edwards, "Magnetic metamaterials as 1-d data transfer channels: an application for magneto-inductive waves," *IEEE Trans. Microw. Theor. Tech.*, vol. 58, no. 5, pp. 1248–1256, 2010.
[13] Z. Sun and I. F. Akyildiz, "Magnetic induction communications for wireless underground sensor networks," *IEEE Trans. Antennas Propag.*, vol. 58, no. 7, pp. 2426–2435, 2010.
[14] B. Gulbahar and O. B. Akan, "A communication theoretical modeling and analysis of underwater magneto-inductive wireless channels," *IEEE Trans. Wireless Commun.*, vol. 11, no. 9, pp. 3326–3334, 2012.
[15] W. Zhong, C. K. Lee, and S. Y. R. Hui, "General analysis on the use of Tesla's resonators in domino forms for wireless power transfer," *IEEE Trans. Ind. Electron.*, vol. 60, no. 1, pp. 261–270, 2011.
[16] J. I. Agbinya, "A magneto-inductive link budget for wireless power transfer and inductive communication systems," *Prog. Electromagn. Res C*, vol. 37, pp. 15–28, 2013.
[17] C. J. Stevens, "A magneto-inductive wave wireless power transfer device," *Wirel. Power Transf.*, vol. 2, no. 1, pp. 51–59, 2015.
[18] Y. Chen, S. Munukutla, P. Pasupathy, D. P. Neikirk, and S. L. Wood, "Magneto-inductive waveguide as a passive wireless sensor net for structural health monitoring," *Proc. SPIE*, vol. 7647, p. 764749, 2010.
[19] T. Floume, "Magneto-inductive conductivity sensor," *Metamaterials*, vol. 5, no. 4, pp. 206–217, 2011.
[20] R. R. A. Syms, I. R. Young, M. M. Ahmad, and M. Rea, "Magnetic resonance imaging using linear magneto-inductive waveguides," *J. Appl. Phys.*, vol. 112, no. 11, p. 114911, 2012.
[21] R. R. A. Syms, L. Solymar, I. R. Young, and T. Floume, "Thin-film magneto-inductive cables," *J. Physics D: Appl. Phys.*, vol. 43, no. 5, p. 055102, 2010.
[22] R. R. A. Syms, L. Solymar, and I. R. Young, "Broadband coupling transducers for magneto-inductive cables," *J. Phys. D: Appl. Phys.*, vol. 43, no. 28, p. 285003, 2010.
[23] E. Weber, *Electromagnetic theory*. New York: Dover, 1965.
[24] M. Misakian, "Equations for the magnetic field produced by one or more rectangular loops of wire," *J. Res. Natl. Inst. Stand. Technol.*, vol. 105, pp. 557–564, 2000.